Small-scale structure in the interstellar medium: time-varying interstellar absorption towards κ Velorum

Keith T. Smith,[1][*][†] Stephen J. Fossey,[2] Martin A. Cordiner,[1,3] Peter J. Sarre,[1] Arfon M. Smith,[1,4] Tom A. Bell[5,6] and Serena Viti[2]

[1]*School of Chemistry, The University of Nottingham, University Park, Nottingham NG7 2RD*
[2]*Department of Physics and Astronomy, University College London, Gower Street, London WC1E 6BT*
[3]*Astrochemistry Laboratory and The Goddard Center for Astrobiology, Mailstop 691, NASA Goddard Space Flight Center, 8800 Greenbelt Road, Greenbelt, MD 20770, USA*
[4]*Department of Physics, University of Oxford, Oxford OX1 3RH*
[5]*Department of Astronomy, California Institute of Technology, Pasadena, CA 91125, USA*
[6]*Centro de Astrobiología (CSIC-INTA), 28850 Madrid, Spain*

ABSTRACT

Ultra-high spectral resolution observations of time-varying interstellar absorption towards κ Vel are reported, using the Ultra-High Resolution Facility on the Anglo-Australian Telescope. Detections of interstellar Ca I, Ca II, K I, Na I and CH are obtained, whilst an upper limit on the column density is reported for C_2. The results show continued increases in column densities of K I and Ca I since observations $\sim$4 yr earlier, as the transverse motion of the star carried it $\sim$10 au perpendicular to the line of sight. Line profile models are fitted to the spectra and two main narrow components (A and B) are identified for all species except CH. The column density $N(\text{K I})$ is found to have increased by 82^{+10}_{-9} per cent between 1994 and 2006, whilst $N(\text{Ca I})$ is found to have increased by 32 ± 5 per cent over the shorter period of 2002–2006. The line widths are used to constrain the kinetic temperature to $T_{k,A} < 671^{+18}_{-17}$ K and $T_{k,B} < 114^{+15}_{-14}$ K. Electron densities are determined from the Ca I/Ca II ratio, which in turn place lower limits on the total number density of $n_A \gtrsim 7 \times 10^3$ cm^{-3} and $n_B \gtrsim 2 \times 10^4$ cm^{-3}. Calcium depletions are estimated from the Ca I/K I ratio. Comparison with the chemical models of Bell et al. confirms the high number density, with $n = 5 \times 10^4$ cm^{-3} for the best-fitting model. The first measurements of diffuse interstellar bands (DIBs) towards this star are made at two epochs, but only an upper limit of $\lesssim$40 per cent is placed on their variation over $\sim$9 yr. The DIBs are unusually weak for the measured $E(B - V)$ and appear to exhibit similar behaviour to that seen in Orion. The ratio of equivalent widths of the λ5780 to λ5797 DIBs is amongst the highest known, which may indicate that the carrier of λ5797 is more sensitive to ultraviolet radiation than to local density.

Key words: ISM: atoms – ISM: individual objects: κ Vel cloud – ISM: lines and bands – ISM: molecules – ISM: structure – local interstellar matter.

1 INTRODUCTION

Over the past two decades an increasing body of observational evidence has indicated that the diffuse interstellar medium (ISM) is highly structured on scales below 1 pc, contrary to earlier theoretical expectations (McKee & Ostriker 1977) and observations which had suggested an apparent minimum cloud size (e.g. Crovisier,

Kazes & Dickey 1985). Evidence for small-scale structure (SSS) has come from observations of interstellar absorption at radio, optical and ultraviolet (UV) wavelengths along closely separated lines of sight. Such sightlines have been provided by spatially resolved observations of extended extragalactic radio sources (Dieter, Welch & Romney 1976; Diamond et al. 1989; Lazio et al. 2009), binary stars (Meyer 1990; Watson & Meyer 1996; Cordiner et al. 2006) and star clusters (Andrews, Meyer & Lauroesch 2001; van Loon et al. 2009). Alternatively, a single background source can be observed repeatedly over several years, with each epoch probing a slightly different line of sight due to the transverse proper motion of the source and/or the intervening interstellar material. This

---

[*] E-mail: kts@ras.org.uk
[†] Present address: Royal Astronomical Society, Burlington House, Piccadilly, London W1J 0BQ.

technique has been applied to radio observations towards pulsars (Frail et al. 1994; Stanimirović et al. 2003, 2010) and optical observations towards nearby early-type stars (e.g. Blades et al. 1997; Price, Crawford & Barlow 2000; Danks et al. 2001; Welty 2007; see also the review by Crawford 2003). These observations indicate that large differences in column density can exist between lines of sight with transverse separations from as few as tens to thousands of au.

Heiles (1997) considered possible theoretical scenarios to explain these variations without grossly violating pressure equilibrium with the surrounding ISM. His preferred model consisted of a population of cold and relatively dense structures in the form of sheets or filaments; the observed variations could then be produced if a structure was present and closely aligned to the line of sight. The model required very low temperature gas ($\sim$15 K) to maintain pressure equilibrium. However, evidence for such a low temperature has not been found; instead, more recent observations have indicated that a small but significant fraction of diffuse gas is at high pressure (Jenkins & Tripp 2001, 2011). Heiles & Stinebring (2007) have summarized the observational and theoretical constraints on models for SSS, and theoretical attention has now shifted towards solutions which do not require dynamical equilibrium (e.g. Heiles 2007). Such overpressured clouds are expected to evaporate quickly, so a mechanism (e.g. magnetohydrodynamic waves, as discussed by Hartquist, Falle & Williams 2003) must be invoked to replenish the population of small-scale structures.

The existence of small-scale relatively dense regions within the diffuse ISM has important implications for interstellar chemistry. Although the interstellar radiation field is expected to be essentially unattenuated within such structures, the high density can result in enhancement of the molecular content (Bell et al. 2005). This provides a potential method for obtaining new information on the physical conditions, and a possible solution to some of the challenges which exist in reproducing the abundances of molecules observed along lines of sight through the diffuse ISM (Cecchi-Pestellini et al. 2009). A comprehensive understanding of the physical conditions within the SSS is required, so that it may be fed into such chemical models.

This paper is organized as follows. In Section 2, we describe previous studies of SSS towards κ Vel, whilst our observations are detailed in Section 3. The results are presented in Section 4, along with a line profile analysis. Section 5 contains a comparison with earlier observations and a discussion of the physical and chemical conditions towards κ Vel. Conclusions are presented in Section 6.

2 BACKGROUND

κ Velorum (HD 81188) is a bright $V = 2.46$ single-lined spectroscopic binary star with an orbital amplitude of 46.5 km s^{-1} and period of 117 d (Pourbaix et al. 2004); the spectral type of the primary is B2 IV, whilst the nature of the secondary is unknown. The distance to the system obtained from its trigonometric parallax measured by the *Hipparcos* satellite is 165 ± 13 pc (Perryman 1997);[1] the reddening is $E(B - V) = 0.10$ mag (Cha et al. 2000). Early

high-resolution observations of the ISM towards this star taken in 1989 and 1994 have been presented by Crawford (1991) and Dunkin & Crawford (1999), respectively.

Small-scale structure towards κ Vel was first noted by Crawford et al. (2000), who serendipitously discovered that the equivalent width of the interstellar K I line had increased by $\sim$40 per cent between 1994 and 2000, with a corresponding but smaller increase in absorption by Na I. The enhancement was found to be in a single narrow ($b = 0.24$ km s^{-1}) absorption component located at a velocity[2] $v_\odot = +8.5$ km s^{-1}. The observations were interpreted as indicating that as the proper motion of κ Vel carried it $\sim$15 au tangentially between 1994 and 2000 the line of sight gradually intercepted a filament of cold and/or dense material aligned along the line of sight, of the type proposed by Heiles (1997).

Follow-up observations by Crawford (2002) detected Ca I and CH absorption at the same velocity, and found a continued increase in the K I column density. From a consideration of the Ca I/Ca II ratio, CH abundance and stellar proper motion, Crawford (2002) concluded that the absorbing material lay in a cool ($T \sim 100$ K), dense ($n_H \gtrsim 10^3$ cm^{-3}) cloud with approximate dimensions of $100-1000$ au in depth (along the line of sight) and 15 au in the transverse direction.

Consideration of this cloud prompted Bell et al. (2005) to develop a chemical model of such a filament. The column densities of several atomic and molecular species were calculated for a cloud with physical extent similar to that inferred by Crawford (2002) as a function of time, radiation field and density. The models which most closely reproduced the observations towards κ Vel were for a young ($\sim$50 yr), transient (lifetime < 100 yr) and high-density ($n_H \gtrsim 10^4$ cm^{-3}) filament immersed in a typical ambient interstellar radiation field. The models predicted that detectable column densities of additional diatomic molecules could be present, including C_2 and OH.

The line of sight towards κ Vel offers an excellent opportunity to explore the ongoing chemical and dynamical evolution of SSS. We therefore set out to re-observe the chemical species studied by Crawford (2002), and to conduct a search for C_2, in order to further constrain the physical and chemical conditions and test the chemical model of Bell et al. (2005). In particular, detection of the homonuclear molecule C_2 could be used to measure the local kinetic temperature through the populations of each rotational J-state (and radiation temperature and density, if sufficient high-J lines were also detected; cf. van Dishoeck & Black 1982). The resolved intrinsic profiles of the narrow interstellar lines could then be used to infer the turbulent contribution to the line widths (Crawford 1997), which could be particularly important for understanding the origin and evolution of SSS.

3 OBSERVATIONS

Observations of interstellar absorption towards κ Vel were made on the nights of 2006 March 9–15 using the Ultra-High Resolution Facility (UHRF; Diego et al. 1995) located at the coudé focus of the 3.9 m Anglo-Australian Telescope (AAT). The UHRF is an echelle spectrograph which is capable of ultra-high resolution but can only record simultaneous data over a very narrow wavelength region, so a separate set-up is required for each species. A summary of the observations is presented in Table 1. New observations of

---

[1] van Leeuwen (2007) presented an updated reduction of the *Hipparcos* data with significantly improved astrometry for most stars. However, in the case of κ Vel the new reduction resulted in a 'stochastic' solution as opposed to the fully converged solution found in 1997. The distances and proper motions calculated from the two reductions are consistent to within their mutual error bars. For this particular star, we have therefore chosen to adopt the astrometry from Perryman (1997).

[2] All velocities quoted in this paper are heliocentric. To convert to local standard of rest velocities towards κ Vel subtract 11.43 km s^{-1}.

Table 1. Summary of the UHRF observations towards κ Vel. Exp time is the total exposure time, S/N is the resulting per-pixel continuum signal-to-noise ratio and W is the equivalent width integrated over the entire velocity profile. Errors are 1σ. The C_2 upper limit is 3σ on each of the five lines which fall in the observed wavelength region.

	UT date	Exp time (h)	S/N	W (mÅ)
Ca I	2006 March 10	4.0	380	1.13 ± 0.02
Ca II	2006 March 11	0.5	160	23.24 ± 0.26
K I	2006 March 09,10	2.75	210	7.49 ± 0.34
Na I	2006 March 11	0.67	190	60.18 ± 0.14
CH	2006 March 09,11	9.0	600	0.25 ± 0.03
C_2	2006 March 12–15	15.0	800	< 0.11

the absorption lines due to Ca I, Ca II (K line), K I (7698 Å line) and Na I (D_1 line) were obtained, along with rotational lines of the $A^2\Delta \leftarrow X^2\Pi$ (0,0) band of the CH molecule in the $R_2(1)$ Λ-doublet [comprising the $R_{fe}(1/2)$ and $R_{ff}(1/2)$ lines]. A search was performed for the C_2 molecule in several low-J lines [R(0), Q(2), Q(4), Q(6) and P(2)] of the $A^1\Pi_u \leftarrow X^1\Sigma_g^+$ Phillips (2,0) band, which were covered in a single instrumental set-up.

The detector used for the atomic lines and CH was the blue-optimized EEV2 CCD (2048 × 4096 13.5-μm pixels). The EEV2 was operated in normal readout mode, which provides an RMS readout noise of 3.2 e$^-$ pixel^{-1} and an unbinned readout time of 180 s. Because the image slicer (see below) projects the spectrum on to ∼1400 unbinned pixels, the EEV2 was binned by a factor of eight perpendicular to the dispersion to reduce the readout noise and time. The EEV2 CCD suffers from severe fringing at wavelengths above ∼6500 Å, which particularly affected the K I observations, necessitating careful flat-fielding. For the C_2 observations, the red-optimized MITLL3 CCD (2048 × 4096 15-μm pixels) was used due to its higher quantum efficiency and lower fringing at long wavelengths. As the MITLL3 detector could not be binned, it was operated in slow readout mode, which provides a readout noise of 1.8 e$^-$ pixel^{-1} and a readout time of 300 s.

The UHRF was operated in '$R = 1E6$' mode, the highest spectral resolution available, which is vital to study the profiles of narrow interstellar lines. Wavelength calibration used a Th–Ar arc lamp, whilst flat-fields were obtained with an internal quartz–halogen calibration lamp. In this resolution mode, the instrument resolves the lines from the arc lamp, so a stabilized He–Ne laser was used to measure the instrumental resolution. The resolving power ($R \equiv \lambda/\Delta\lambda$) was found to be $R \simeq 845\,000$ for the EEV2 and $R \simeq 940\,000$ for the MITLL3, corresponding to velocity resolutions of 0.355 and 0.319 km s^{-1}, respectively.

Individual exposures were limited to 30 min to prevent degradation of the instrumental resolution by the changing heliocentric velocity correction due to the rotation of the Earth. The detector readout times therefore constituted a significant overhead, and detector readout noise made a small but significant contribution to the overall noise level.

The UHRF incorporates an image slicer which reformats a 1.5″ × 1.5″ entrance aperture to a 0.06 arcsec slit to reduce slit losses, but itself has a peak throughput of only 15 per cent. Observing conditions were clear on the nights of March 9 and 15, but those of March 10–14 were frequently interrupted by cloud and fog. The seeing during the observations varied in the range 1–3 arcsec, mostly around 1.5 arcsec.

Data reduction was performed using the `noao.onedspec` routines in IRAF.[3] Pixel-to-pixel sensitivity variations and fringing were removed by division by a normalized flat-field. The scattered light background was measured from the inter-order regions and subtracted. The Na I, Ca I, K I, CH and C_2 observations were corrected for telluric absorption by division by a well-exposed spectrum of a bright, fast-rotating, early-type standard star (α Vir and/or α Eri); the Ca II observations were found to be free of telluric contamination. Individual exposures were converted to a heliocentric reference frame before being co-added and converted to a velocity scale.

Additional observations of diffuse interstellar bands (DIBs; see the review by Sarre 2006) were obtained using other spectrographs at two additional epochs. The earlier observations were obtained during 1995 January as part of a survey of DIBs towards southern stars conducted by one of us (SJF). The instrument used was the coudé echelle spectrograph on the 74-inch telescope at the Mount Stromlo Observatory. The resolving power was $R \simeq 60\,000$ and the signal-to-noise ratio (S/N) was ∼550. Later observations were obtained during 2004 June, as part of a larger study of DIBs as tracers of SSS (Cordiner et al. 2006; Cordiner et al., in preparation). The instrument used was the University College London Echelle Spectrograph (UCLES) on the AAT. The spectral resolution was $R \simeq 58\,000$ and the S/N was ∼2300. Full details of the observations and data reduction have been given by Cordiner (2006) and Cordiner et al. (2006). The 1995 and 2004 data were corrected for telluric absorption using composite spectra obtained by co-adding spectra of the same two stars (α Vir and α Eri), observed at both epochs. These telluric standards were obtained at similar airmasses to κ Vel and required negligible intensity scaling, so any residual stellar features should be the same at both epochs.
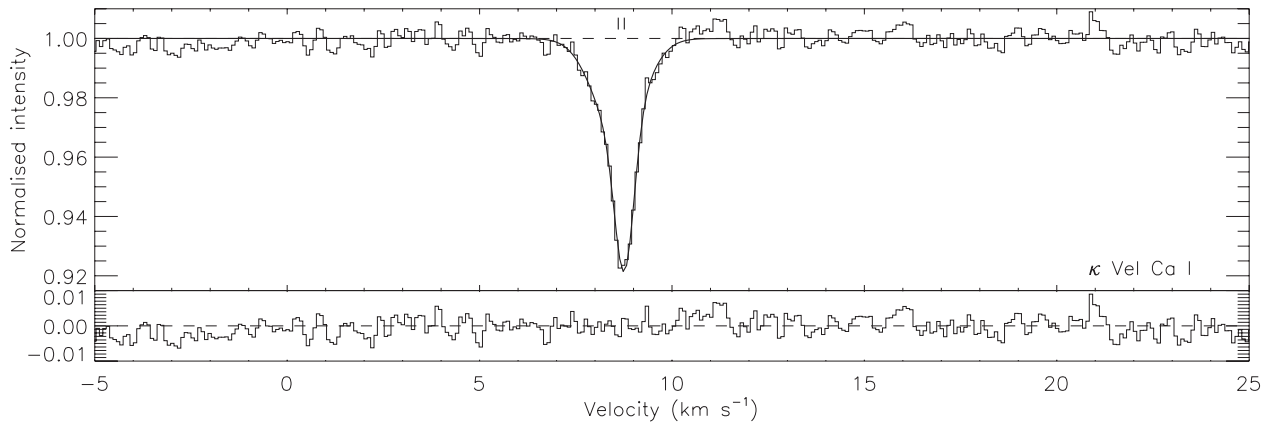
4 RESULTS AND LINE PROFILE ANALYSIS

High S/N was achieved in the UHRF observations of each line, improving upon the earlier observations of Crawford (2002) by factors of 1.5–2 in S/N. All of the atomic absorption lines were detected at high significance. Absorption by the CH molecule was also found but none of the C_2 lines were detected, for which we determined upper limits. The UHRF spectra are shown in Figs 1–5; the continuum S/N values and measured total equivalent widths are given in Table 1. Preliminary results from these observations were presented by Smith (2010); they are superseded by the results presented here.

The line profiles of the detected species were modelled using the VAPID interstellar line modelling program (Howarth et al. 2002), which computes the optimum column density N, velocity v and Doppler broadening parameter[4] b for a given set of absorption components using a non-linear χ^2 minimization algorithm. Individual absorption components have a Voigt profile formed by the convolution of the Lorentzian natural line shape, the instrumental point spread function (PSF; taken to be Gaussian with widths given by the velocity resolution found in Section 3) and a Gaussian with broadening parameter b.
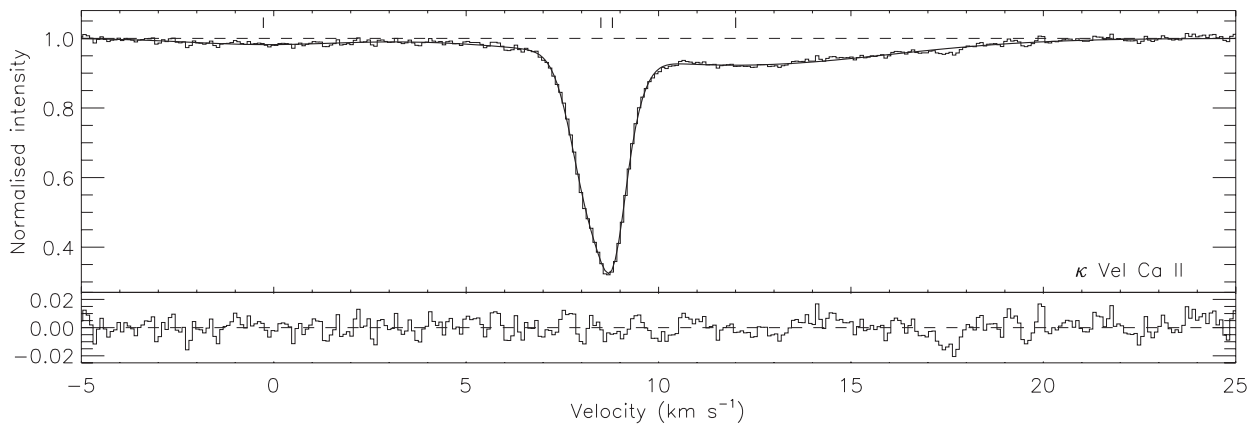
The wavelengths and oscillator strengths adopted in the analysis are given in Table 2, and were taken from Morton (2003)

---

[3] IRAF is distributed by the National Optical Astronomy Observatories, which are operated by the Association of Universities for Research in Astronomy, Inc., under cooperative agreement with the National Science Foundation.
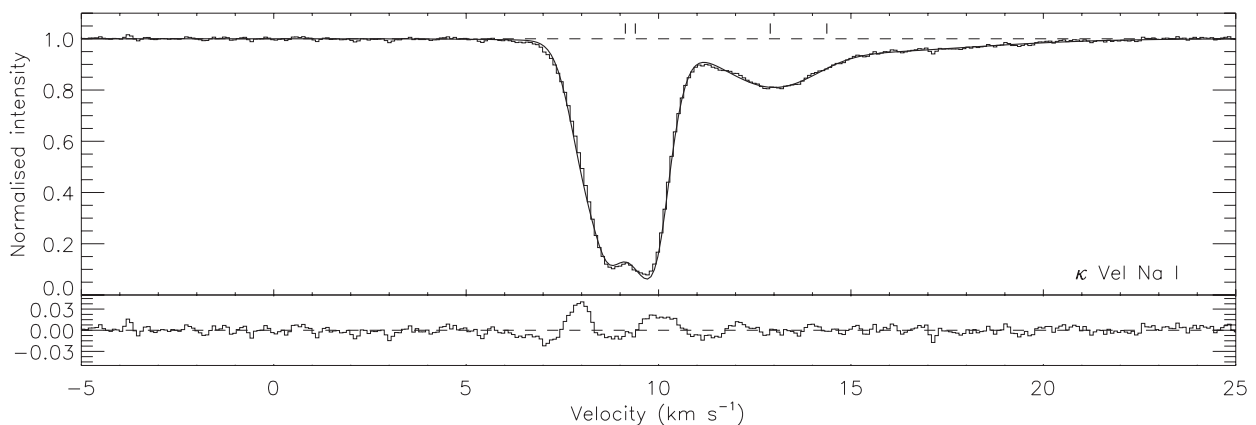
[4] The broadening parameter b is related to the full width at half-maximum (FWHM) of the corresponding Gaussian distribution by $b = \text{FWHM}/2\sqrt{\ln 2}$.

Figure 1. Interstellar Ca I absorption observed towards κ Vel. In the upper panel, the thin histogram is the observed spectrum and the thick line is the fitted model profile. The lower panel shows the residuals. The dashed line indicates the continuum level and tick marks indicate the positions of each absorption component listed in Table 3. The velocity scale is heliocentric.
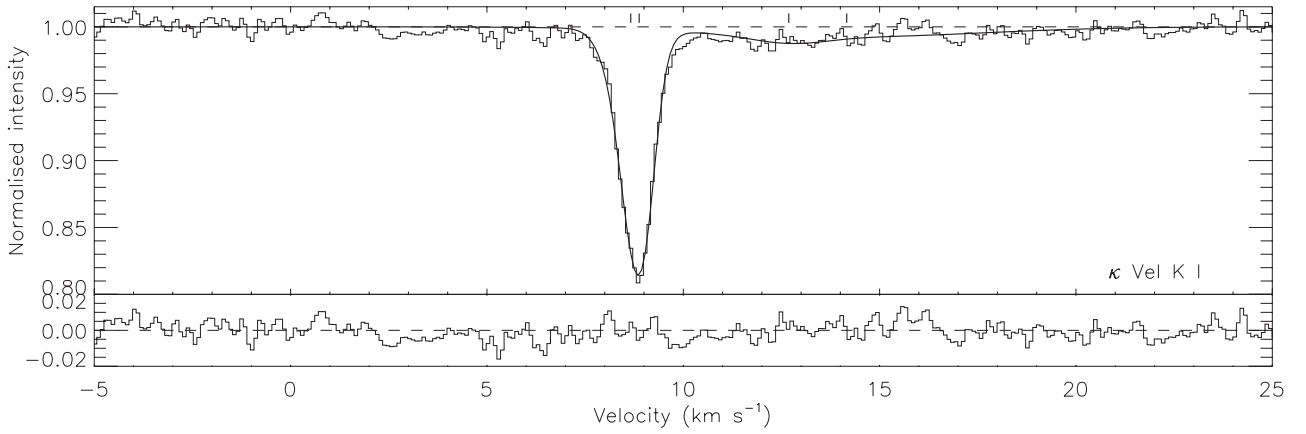

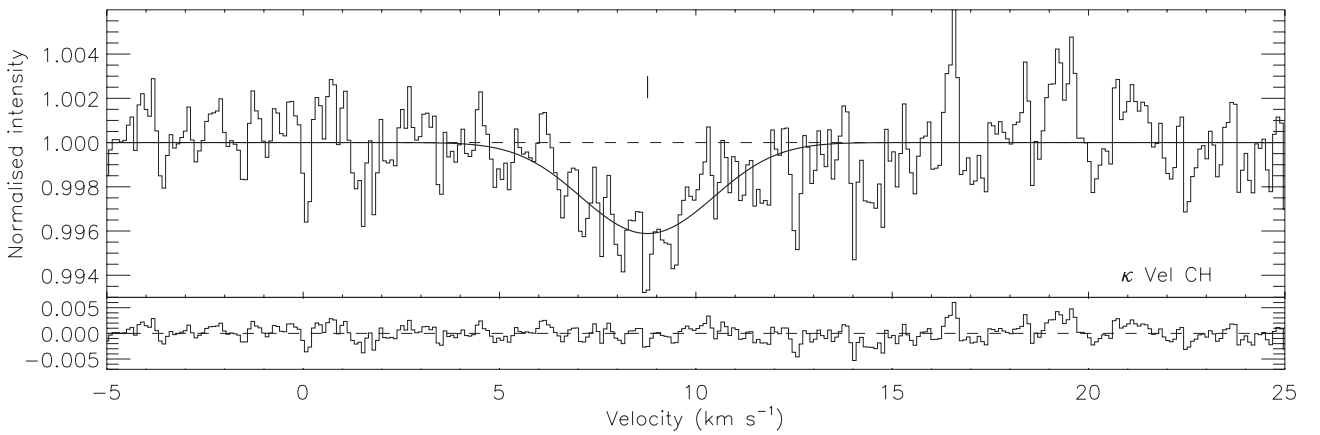**Figure 2.** As in Fig. 1, but for interstellar Ca II K absorption.

Figure 3. As in Fig. 1, but for interstellar Na I D_1 absorption. The model does not completely fit the core of the line (see Section 4.2.3).

for the atomic species, Black & van Dishoeck (1988) for CH and Sonnentrucker et al. (2007) for C_2. The CH rotational lines form a Λ-doublet split by 1.43 km s^{-1}; the velocities output by VAPID are with respect to the bluest transition, and were converted to the weighted mean of the two lines by subtraction of 0.72 km s^{-1}. The two levels which contribute to the doublet were assumed to have equal populations, because the energy splitting between them is negligibly small compared to the thermal energy (cf. Crane, Lambert & Sheffer 1995); the oscillator strengths used in

VAPID were apportioned accordingly. The K I and Na I D_1 transitions are split by nuclear hyperfine structure, resulting in two lines 0.370 and 1.083 km s^{-1} apart, respectively. The relative strengths of the transitions are equal to $2F + 1$, which for both observed Na I and K I transitions gives a ratio of 5:3 with the stronger transition being the redder of the pair (see Welty, Hobbs & Kulkarni 1994 or Morton 2003 for derivations). The VAPID output velocities were converted to the weighted mean velocity of the transitions by subtraction of 0.231 and 0.677 km s^{-1} for K I

Figure 4. As in Fig. 1, but for interstellar K I absorption.

Figure 5. As in Fig. 1, but for interstellar CH absorption.

Table 2. Atomic and molecular line data adopted in the line profile analysis. Wavelengths and oscillator strengths f are taken from Morton (2003) for the atomic species, Black & van Dishoeck (1988) for CH and Sonnentrucker et al. (2007) for C_2. The Na I and K I lines have hyperfine structure, whilst C_2 and CH each have several rotational lines. Oscillator strengths have been apportioned between hyperfine components in a 5:3 ratio according to the prescriptions of Welty et al. (1994). For C_2, the line ratios given by Sonnentrucker et al. (2007) have been adopted.

		Wavelength (Å)	f
Ca I		4226.728	1.77
Ca II K		3933.6614	6.267×10^{-1}
K I		7698.9586	1.248×10^{-1}
		7698.9681	2.079×10^{-1}
Na I D_1		5895.9109	1.200×10^{-1}
		5895.9322	2.001×10^{-1}
CH	$R_{ff}(1/2)$	4300.3235	2.53×10^{-3}
	$R_{fe}(1/2)$	4300.3030	2.53×10^{-3}
C_2	R(0)	8757.686	1.40×10^{-3}
	Q(2)	8761.194	7.0×10^{-4}
	Q(4)	8763.751	7.0×10^{-4}
	Q(6)	8767.759	7.0×10^{-4}
	P(2)	8766.031	1.4×10^{-4}

and Na I, respectively. For each C_2 J-state, the oscillator strength was apportioned between the P, Q and R branches according to the relative line strengths given by Sonnentrucker et al. (2007). The results of the fitting are presented in Table 3.

4.1 Uncertainties

The results of the line profile analysis are affected by a number of sources of uncertainty, both statistical and systematic. Rigorous estimates of the statistical uncertainty were obtained by generating 1000 Monte Carlo noise simulations for each line, in which Gaussian noise corresponding to the measured S/N was added to the data and the fits repeated. The lower S/N present in the cores of the lines due to the fewer photons detected was taken into account during the Monte Carlo process, under the assumption of Poisson statistics. Statistical uncertainties are given in Table 3.

In addition to these statistical uncertainties, there are a number of systematic uncertainties, primarily affecting the measured velocities. The small wavelength coverage of the UHRF (4–9 Å) results in only a low number of arc lines for wavelength calibration, which limits the absolute precision, particularly in the case of C_2 for which only four arc lines were available. The magnitude of this effect can be estimated from the RMS of the wavelength fit (which used a cubic polynomial, quadratic for C_2), which was always less than 0.01 km s^{-1}. Uncertainties in the atomic data listed in Table 2 may affect the velocities, e.g. the wavelength of the Ca II K line is known to be uncertain by about 0.02 km s^{-1} (Morton 2003). Velocity shifts *between* observations of a few tenths of a km s^{-1}

Table 3. Results of the line profile analysis of the UHRF observations of interstellar absorption towards κ Vel. The heliocentric velocity $v_\odot$, Doppler broadening parameter b and logarithm of the column density N (in cm^{-2}) are given for each model component. The total convolved line profiles are plotted in Figs 1–5. T_k^{ul} is the upper limit on the kinetic temperature calculated from equation (1) assuming no turbulent contribution to the b value (see Section 5.2). Heliocentric velocities are quoted with respect to the weighted means of the transitions for each species. Statistical uncertainties are quoted as 1σ.

	$v_\odot$ (km s^{-1})	b (km s^{-1})	log N	T_k^{ul} (K)
Ca I	8.604 ± 0.033^A	0.851 ± 0.049	9.412 ± 0.032	1760^{+210}_{-200}
	8.762 ± 0.011^B	0.268 ± 0.025	9.198 ± 0.051	174^{+34}_{-31}
Ca II	-0.27 ± 0.18	2.81 ± 0.21	10.123 ± 0.033	–
	8.500 ± 0.005^A	0.755 ± 0.006	11.240 ± 0.005	1381^{+22}_{-22}
	8.802 ± 0.007^B	0.283 ± 0.012	10.521 ± 0.024	194^{+17}_{-16}
	12.003 ± 0.068	5.516 ± 0.086	11.078 ± 0.006	–
K I	8.200 ± 0.017^A	0.609 ± 0.036	10.141 ± 0.014	880^{+110}_{-100}
	8.414 ± 0.008^B	0.346 ± 0.017	10.234 ± 0.009	283^{+28}_{-27}
	12.225^f	1.31^f	9.30 ± 0.12	–
	13.70^f	4.86^f	9.979 ± 0.050	–
Na I	8.460 ± 0.007^A	0.694 ± 0.009	11.887 ± 0.009	671^{+18}_{-17}
	8.720 ± 0.008^B	0.286 ± 0.018	11.327 ± 0.032	114^{+15}_{-14}
	12.225 ± 0.039	1.31 ± 0.11	10.933 ± 0.053	–
	13.70 ± 0.71	4.86 ± 0.55	11.007 ± 0.092	–
CH	8.77 ± 0.23	2.06 ± 0.56	11.470 ± 0.051	–

^{A}Component A, ^{B}component B,
^{f}values held fixed during fitting (see Section 4.2.4).

have been seen in previous UHRF data (e.g. Crawford et al. 2000) and are thought to result from slight differences between the light paths of the telescope and arc lamp beams. The slight velocity offsets between the velocity components found in this work and those found by Crawford et al. (2000) are of similar magnitude. The quoted velocities are therefore systematically uncertain at around this level. Nevertheless, the multiple components for each species should be affected in an identical fashion by this systematic uncertainty, so the *relative* velocities between components of a single species are unaffected, and so we do not incorporate this systematic uncertainty into Table 3.

Another potential source of systematic uncertainty is the definition of the continuum level. With the exception of Ca II (see Section 4.2.2), there are no stellar counterparts to the interstellar lines. Around a thousand pixels of clear continuum were present on both sides of every observed line. This greatly eases determination of the continuum level, which was fitted with a low-order polynomial (quadratic or cubic). The uncertainty in the continuum level is therefore negligible compared to the statistical uncertainties.

Finally, we consider the systematic uncertainty introduced by the determination of the instrumental PSF. Inspection of the He–Ne laser and Th–Ar arc lamp spectra shows no evidence for a non-Gaussian PSF. The measurement of the width of the PSF (and hence instrumental resolution) carries an uncertainty of $\sim$0.001 km s^{-1}, which translates to a systematic uncertainty of $\sim$0.0006 km s^{-1} on the measured b values. This uncertainty is negligibly small compared to the statistical uncertainties on b, and affects all model components equally, so it has not been included in the uncertainties quoted in Table 3.

4.2 Atomic species

Previous observers have modelled the main absorption around 9 km s^{-1} with either one or two separate components. Dunkin & Crawford (1999) and Crawford et al. (2000) found that their K I and Na I data required two components, whilst Crawford (2002) modelled only a single component in Ca I and CH (but noted that these line profiles would also be consistent with the presence of two components, as found for the stronger lines). Whilst modelling the atomic species, it was found that a two-component model fitted to the narrower $\sim$9 km s^{-1} feature was significantly better than a one-component model for all atomic species. This was confirmed through examination of the fit residuals and via a statistical F-test, which found that the two-component model was statistically better (in the sense of improvement in χ^2) at at least the 95 per cent confidence level. The similarities in the velocities and b values obtained for each species, which were derived independently (except for K I, see Section 4.2.4), reinforce the interpretation that a two-component model is justified by the new high S/N data.

For each atomic species, the main absorption around 9 km s^{-1} contains a narrow component at $v \sim 8.5$ km s^{-1} with $b \sim 0.7$ km s^{-1} (hereafter component A), and a slightly higher velocity and even narrower component at $v \sim 8.7$ km s^{-1} with $b \sim 0.3$ km s^{-1} (component B). These components are consistent with the previously reported two-component b values of Crawford et al. (2000), though at slightly shifted velocity. All of the atomic species except Ca I also include a broader absorption around $\sim$12 km s^{-1}; this absorption was seen in Ca II and K I by Crawford (2002), but only included in his Ca II model. The methodology adopted in modelling each species is described in more detail below.

4.2.1 Ca I

There is no evidence for broad components in the Ca I absorption, so the model consists of the narrow components A and B only (see Fig. 1). Although the absorption only reaches a depth of 8 per cent of the continuum, the high S/N data confirm the need for two narrow components.

4.2.2 Ca II

Calcium K is the only observed line which has a photospheric counterpart. The rotational velocity of κ Vel is $v_{rot} \sin i = 55$ km s^{-1} (Głębocki & Stawikowski 2000), so the stellar line is much broader than the interstellar features. Fortuitously, the orbital motion of the spectroscopic binary during our observations resulted in displacement of the stellar line to a velocity well clear of the interstellar absorption. In contrast to previous observations, the stellar line does not overlap the interstellar features in our data, which makes the continuum definition straightforward. The narrow absorption around 9 km s^{-1} clearly requires two components in the model (see Fig. 2). The broad higher velocity absorption has been modelled with a single $b = 5.516 \pm 0.086$ km s^{-1} component [Crawford (2002) also modelled this as a single component]. There is no evidence for two broad components as found for Na I (see Section 4.2.3 below). A new Ca II absorption component at about 0 km s^{-1} is also found, which was regarded as part of the stellar continuum by Crawford (2002).

4.2.3 Na I

For this species, it was found that two broad higher-velocity cloud components were required in addition to the two narrow

components A and B (see Fig. 3). These components were also found by Crawford et al. (2000), though the parameters of the broad components differ in detail, typically at the 2σ level (but less so when compared to the 1994 observations). Our 12 km s^{-1} component is slightly narrower and weaker, and our 14 km s^{-1} component stronger and broader, than Crawford et al.'s corresponding components; however, the total column density of the two broad components has in fact changed very little between 1994, 2000 and 2006. Given their marginal significance, we therefore consider that the small differences between the modelled broad components might simply be due to the covariance between the fitted parameters, given the difficulty in defining accurately the velocities of such broad overlapping components. If the ~ 14 km s^{-1} component is instead fixed to the velocity found by Crawford et al. (2000), all other fitted parameters become quite consistent with the other epochs, for both broad components. There is therefore no evidence that these broad components are varying between epochs.

There remains a slight discrepancy between the Na I model and data at the core of the narrow components, indicating that further substructure may be present. However, models with additional components did not improve the fit, because the (superposed) blueward hyperfine component within the line cannot be reproduced without the redward hyperfine component becoming too deep relative to the data. An investigation was undertaken to determine whether this behaviour could be explained by an error in the zero-point of the spectrum, but adjusting the level of the zero-point did not improve the fit.

4.2.4 K I

For potassium, a broad high-velocity absorption is visible (Fig. 4). This can be adequately modelled with a single component, but with a very high b value (~ 7 km s^{-1}). However, because this absorption is seen to consist of two separate components in Na I, which is expected to be similarly distributed to K I (Pan et al. 2005), we have chosen to reproduce these two components in the K I model. Although the two components do not result in a statistically significant improvement in the fit, the two-component model is more physically plausible, given the Na I model, and avoids depressing the continuum around the narrow components A and B. The broad components in the K I model were fixed at the velocity and b values found for Na I, but were allowed to vary in column density.

In an unconstrained fit, the narrow components (A and B) collapse to the same velocity, and the model becomes inconsistent with the velocity separation seen in the other atomic species. We therefore prefer a model for K I in which the components reproduce the velocity separation seen in earlier observations and in the other species. We iterated towards an acceptable model as follows: first the correlation between the distribution of K I and Na I which was assumed for the broad components was extended to the narrow components. The velocity separation between A and B was constrained to be consistent with both the other species and the two-component K I model of Crawford et al. (2000). When the column densities and b values in the ~ 9 km s^{-1} component were fitted in this model, component A appears to be weaker (log $N_A = 9.99$) than the 1994 value reported by Crawford et al. (2000), with B somewhat stronger (log $N_B = 10.32$). Crawford et al. (2000) found that their results were consistent with only the redward component (B) having varied between 1994 and 2000, so we also fixed the column density of component A to the 1994 value, to obtain the final model presented in Table 3 (the uncertainties on the parameters of component A

were obtained by fixing all other components at their fitted values, so are likely underestimated). In all unconstrained fits, component B is even stronger than tabulated here. However, the total column density in both narrow components (A+B) is identical whichever approach is adopted, so that figure is robust even if the relative strengths remain uncertain.

4.2.5 Comparison between atomic species

Although the two main absorption components are broadly consistent between atomic species, their exact velocities, b values and the velocity separation of the two components are not. These differences are most likely to be due to the systematic uncertainties discussed in Section 4.1. Nevertheless, the *relative* velocities between components of the same species are secure.
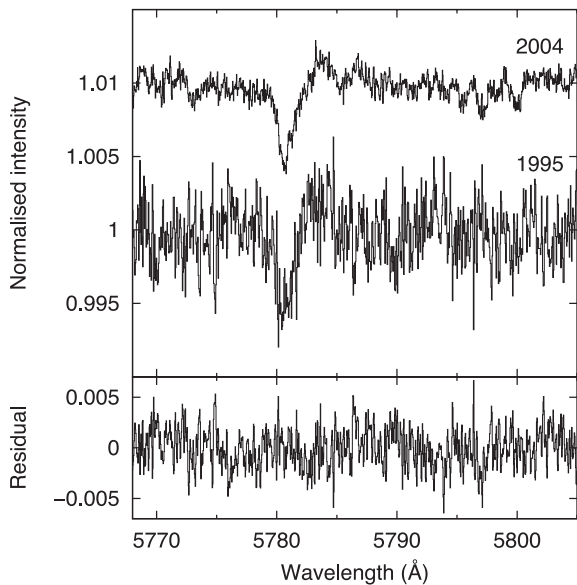
The high-velocity components seen in Na I, K I and Ca II have high b values of up to 5 km s^{-1}. There are three possible explanations for such high b values:

(1) High-temperature gas. We reject this possibility because the temperatures required ($\gtrsim 30\,000$ K) are inconsistent with the presence of substantial amounts of neutral K I and Na I.

(2) Very turbulent gas, with $v_t \gtrsim 4$ km s^{-1}. This would be an unusually high turbulent velocity, but cannot be excluded by the current data.

(3) Multiple blended absorption components, which cannot be distinguished at the current S/N. This seems the most likely explanation (cf. Dunkin & Crawford 1999).

The differences in separation between the narrow components may indicate intrinsic unresolved structure within the absorbing material. Whilst the absorption has been modelled as two components, this does not necessarily imply that there are two physically separate clouds along the line of sight. In particular, the electron and number densities derived in Section 5 are anomalously high for *both* components. There may exist a range of physical conditions within a single 'cloud', which are approximated by the two-component model. The velocity separation between components A and B are larger for Ca II and Na I than for Ca I (and K I). This could potentially be explained if Ca II and Na I are present throughout the cloud, whilst Ca I is present only in the denser regions and K I is intermediate between Na I and Ca I (the distribution of these species in diffuse clouds has been discussed by Pan et al. 2005). If so, the physical parameters derived in Section 5 are indicative of the range of conditions throughout the cloud, but will exclude the most extreme regions. This may also explain the imperfect fit of the model to the core of the Na I line.

4.3 CH

Whilst it might have been expected that CH would have a similar distribution to the atomic species, perhaps with enhancement in the cooler (and presumably denser) component B, no evidence for this has been found. There is no statistical justification for more than one component in the current data. The CH line profile was modelled with a single, broad ($b = 2.06$ km s^{-1}) absorption component, albeit with a high uncertainty ($\sigma_b = 0.56$ km s^{-1}), as shown in Fig. 5. The absorption profile has a central depth of less than 0.5 per cent of the continuum. Although the velocity of the CH absorption is closest to that of component B, the uncertainty and variations between species are large, so CH cannot be conclusively identified with any component seen in the atomic species. We consider the breadth of the CH line profile in more detail in Section 5.3.

Figure 6. Spectra of the region around the λ5780 and λ5797 DIBs recorded towards κ Vel. The upper trace is the observed spectrum in 2004 June, the middle trace is the same region as observed in 1995 January, and the lower trace shows residual intensities of the 2004 minus the 1995 data. The λ5797 DIB is not detected at either epoch, and there is no evidence for temporal variation of the λ5780 DIB.
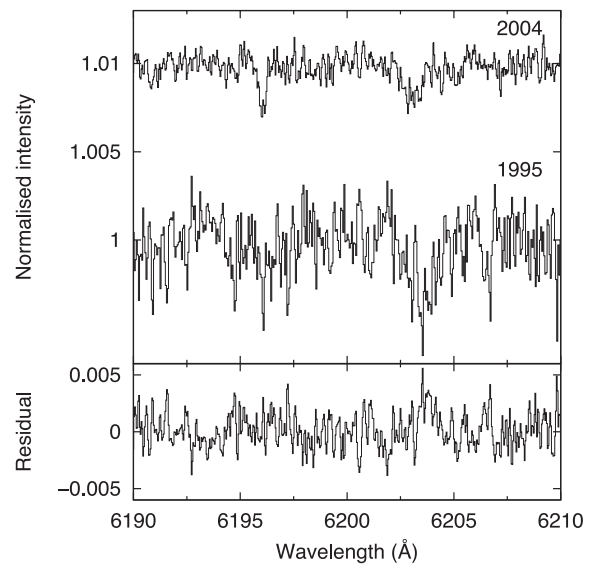
4.4 C_2

The continuum S/N achieved in the region of the C_2 lines was ∼800 but no lines were found. To improve the chances of a detection, the expected positions of the five rotational lines were stacked in velocity space, but this also failed to reveal any absorption. A 3σ upper limit of 0.11 mÅ was determined on each of the five lines. The corresponding upper limit on the total C_2 column density is model dependent; we return to this point in Section 5.8.
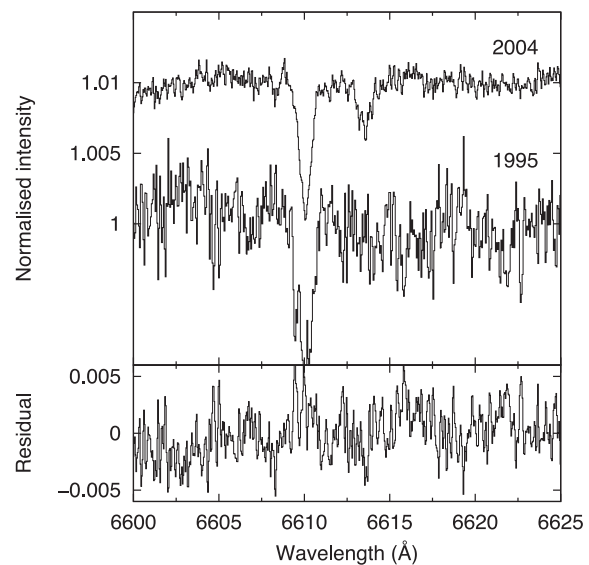
4.5 Diffuse interstellar bands

A search was performed for those DIBs in the observed wavelength regions with potentially detectable equivalent widths, by reference to the survey of DIBs by Hobbs et al. (2008). Five DIBs (λλ5780, 6196, 6203, 6283 and 6613) were detected towards κ Vel in the 2004 data; only λ5780 was detected in the lower S/N 1995 data (see Figs 6–8). As far as the authors are aware, these are the first reported detections of DIBs towards this star, so there are no other epochs for comparison.

The measured DIB equivalent widths are given in Table 4, along with Na I D_1 which was present in both observations, and the K I 7698 line which was within the wavelength coverage in 2004 only. Uncertainties and upper limits were calculated as $\sigma_c \Delta\lambda$, where σ_c is the continuum noise level and $\Delta\lambda$ the DIB FWHM. This simple method is fairly conservative and probably overestimates the uncertainties, particularly for the broadest bands. The λ6283 DIB overlaps the telluric O_2 a-band, which could only be adequately removed from the 2004 data. Blends with stellar lines were determined by reference to the stars υ Sco and α Pav (both B2 IV), which were observed on the same night as the 2004 data. For λ6283, a narrow stellar line at 6287 Å was removed via a Gaussian fit; there are possible weak stellar blends with λ5780 and λ5797. The displace-

Figure 7. As in Fig. 6, but for the λ6196 and λ6203 DIBs. Both DIBs are detected in 2004 only.

Figure 8. As in Fig. 6, but for the λ6613 DIB. The line at 6610 Å is due to stellar N II, whilst the DIB is detected in 2004 only.

ment in the continuum adjacent to λ5780 visible in Fig. 6 is likely to have been introduced as a result of weak stellar features in the telluric standard stars.

As a comparison between the two epochs, the spectra around λ5780 (the only DIB detected at both epochs, and including the region where λ5797 would be expected) were subtracted and the residuals evaluated. This procedure is shown in Fig. 6; within the noise, there has apparently been no change in λ5780 between 1995 January and 2004 June. From the residuals and the uncertainties in the measured equivalent widths, we determine an upper limit on the change in λ5780 between the two epochs of ≲40 per cent.

Table 4. Measured equivalent widths (*W*) of DIBs and atomic lines towards κ Vel in 1995 January and 2004 June. In the final column, 'Y' indicates a definite or probable stellar blend contaminating the DIB, '–' indicates improbable or absent stellar blend and '?' is for indeterminate cases. Uncertainties and upper limits are $\sigma_c \Delta\lambda$.

	W (mÅ)		Blend?
	1995 Jan	2004 June	
λ5780	10 ± 4	10 ± 1	?
λ5797	< 1.5	< 0.4	?
λ5850	< 1.2	< 0.4	–
λ6196	< 0.6	1.1 ± 0.2	–
λ6203	< 6	3 ± 2	–
λ6283	*	19 ± 6	Y
λ6613	< 1.8	3 ± 0.5	–
K I 7698	†	5.5 ± 0.2	–
Na I D_1	60.0 ± 0.3	62.2 ± 0.2	–

*Severe telluric contamination; † outside observed wavelength range.
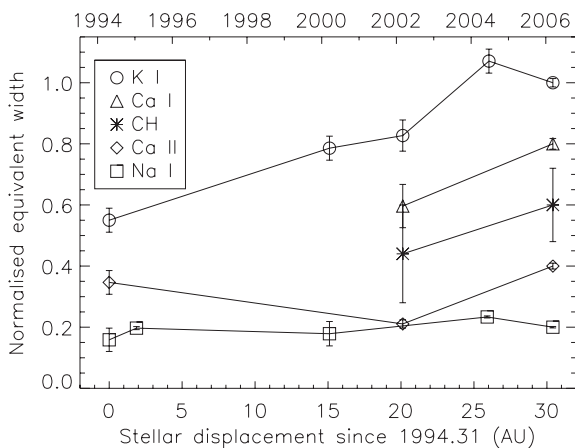
5 DISCUSSION

5.1 Comparison of observations at different epochs

5.1.1 Equivalent widths

A model-independent comparison of the measured equivalent widths of each atomic and diatomic line from all available epochs since 1994 is presented in Fig. 9. For comparison with the earlier measurements from Dunkin & Crawford (1999), Crawford et al. (2000) and Crawford (2002), we have consistently compared equivalent width measurements made over the same velocity range.

For K I, the combined equivalent width of only the narrower ~ 9 km s^{-1} components has been plotted, to be consistent with the earlier data; this was measured as 5.09 ± 0.07 mÅ in the 2006 data by first dividing out the model fit to the broad, higher velocity K I components. These broad components are unavoidably blended with the narrow components in the lower resolution 2004 UCLES
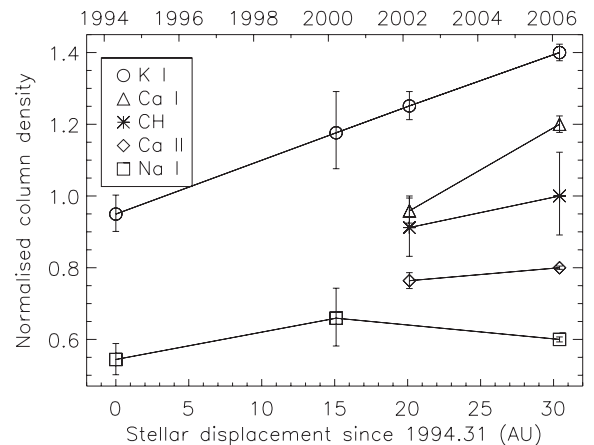
data, leading to that datum appearing too high in Fig. 9. To check this, the 2006 K I observation (including the broad components) was degraded to the same resolution as the 2004 observation, and the equivalent width remeasured. The resulting value was 5.9 mÅ, which is somewhat lower than the total 7.49 mÅ measured from the UHRF data (Table 1) but still higher than the 5.09 mÅ of the narrow components alone. The equivalent width measured at the degraded resolution is thus similar to that measured in the 2004 UCLES data (see Table 4); so the apparently inflated 2004 datum could be an effect of the lower resolution.

There are significant increases in equivalent width for the K I and Ca I lines. W(K I) increased by 82 ± 7 per cent between 1994 and 2006, whilst W(Ca I) increased by 26 ± 9 per cent between 2002 and 2006. The equivalent width of Na I barely changed over the same time periods (4 ± 4 per cent between 1994 and 2006, and 2 ± 4 per cent between 2002 and 2006), although this may be due to the near-saturation of the Na I absorption, which lies on the flat part of the curve of growth. The measured Na I equivalent width also includes the broad, higher velocity components which are not suspected to be variable, given the lack of any significant differences between the models of the 1994, 2000 and 2006 data (see Section 4.2.3). Ca II shows no significant increase (6 ± 4 per cent) in equivalent width between 1994 and 2006, at least when matching velocity components are compared; the 2006 measurement plotted here (20.6 ± 0.2 mÅ) excludes the ~ 0 km s^{-1} component, but the (apparently low) 2002 datum is almost certainly compromised by interference from stellar Ca II K, which was well separated from the interstellar Ca II K line in the 1994 and 2006 data. The increase in CH equivalent width is not statistically significant at 19 ± 22 per cent between 2002 and 2006, but nor are the data inconsistent with CH matching the increases seen in K I and Ca I.

5.1.2 Column densities

The problems caused by the near-saturation of the Na I line and the inclusion of the broad ~ 12 km s^{-1} component may be avoided by instead comparing the modelled column density at each epoch, and restricting comparison to the ~ 9 km s^{-1} component(s) only. This is impractical for the Mount Stromlo and UCLES K I data, in which the narrow and broad components are not resolved, so they are not considered further. The individual (A and B) components

Figure 9. Comparison of observed equivalent widths of interstellar absorbers towards κ Vel at different epochs. Equivalent widths of the interstellar absorption in 1994, 2000 (Crawford et al. 2000), 2002 (Crawford 2002), 1995, 2004 and 2006 (this work) are plotted against stellar displacement on the bottom axis, and epoch in years on the top axis. Data have been normalized with respect to the 2006 values and vertical offsets of 0.2 between species applied for display; lines have been added to guide the eye.

Figure 10. As Fig. 9, but for the combined column density of the interstellar absorption at ~ 9 km s^{-1}. Only the UHRF data from 1994, 2000, 2002 and 2006 are plotted; error bars for 1994 and 2000 are probably overestimates by factors of 5–10 (see Section 5.1.2).

in the UHRF data cannot always be directly compared with the previously published column densities because the absorption has been modelled with different numbers of components (e.g. for Ca I and Ca II). However, all the remaining observations were made with the same instrument at essentially the same spectral resolution (850 000–900 000), and the total column densities (A + B) in the 9 km s^{-1} components are robustly determined.

In Fig. 10, the components reported in Crawford et al. (2000), Crawford (2002) and in this work are compared by summing the column densities of the one or two components which make up the absorption at ∼9 km s^{-1}. Uncertainties in the total column density obtained simply by summing individual components in quadrature are overestimates, because in overlapping lines the column densities of the two components are not independent quantities. The 2002 observations are not affected, because they only utilized one component. For the 2006 observations, the uncertainties were obtained by interrogating the Monte Carlo error simulations, determining the sum of column densities at each iteration, and taking the 68 per cent range. This process revealed a strong anticorrelation between the components, and the total column densities were found to be $\log N_{AB}(\text{Ca I}) = 9.62 \pm 0.01$, $\log N_{AB}(\text{Ca II}) = 11.316 \pm 0.002$, $\log N_{AB}(\text{K I}) = 10.47 \pm 0.01$ and $\log N_{AB}(\text{Na I}) = 11.985 \pm 0.003$. For the 1994 and 2000 observations, only summing in quadrature is possible; by comparison with the 2006 observations, these error bars are likely to be overestimates by factors of 5–10.

The differing treatments of the higher velocity absorption may still affect this comparison. For example, the broad K I components partially overlap the ∼9 km s^{-1} absorption, but were not included in the model of Crawford (2002); this has the effect of slightly enhancing the apparent K I column density in 2002.

Fig. 10 shows that the increase in K I column density first noted by Crawford et al. (2000) has continued until 2006: $N(\text{K I})$ has increased by 82^{+10}_{-9} per cent between 1994 and 2006. For the first time, Ca I is found to have increased – by 32 ± 5 per cent between 2002 and 2006 (a slightly higher rate than K I over the same period). Ca II and CH show no statistically significant changes between 2002 and 2006, and nor does Na I over the period 1994–2006. Ca I and Ca II are therefore seen to vary at different rates to each other, indicating a change in the ionization conditions.

5.2 Line widths and temperature

Although one of the aims of the UHRF observations was to measure the kinetic temperature from the rotational populations of C_2, the lack of a detection of this molecule necessitates the use of another method. In addition to the instrumental resolution and the natural line width, the two mechanisms which act to broaden interstellar lines are thermal Doppler broadening and turbulent bulk motions of the gas. These are related to the Doppler broadening parameter b through

$$b = \sqrt{\frac{2k_B T_k}{m} + v_t^2},$$
(1)

where k_B is the Boltzmann constant, T_k is the kinetic temperature, m is the atomic (or molecular) mass of the species and v_t is the RMS turbulent velocity. Taking the limiting case of zero turbulent velocity, rigorous upper limits on the kinetic temperature T_k^{ul} may be obtained for each species, and are given in Table 3 when $T_k^{ul} < 2000$ K.
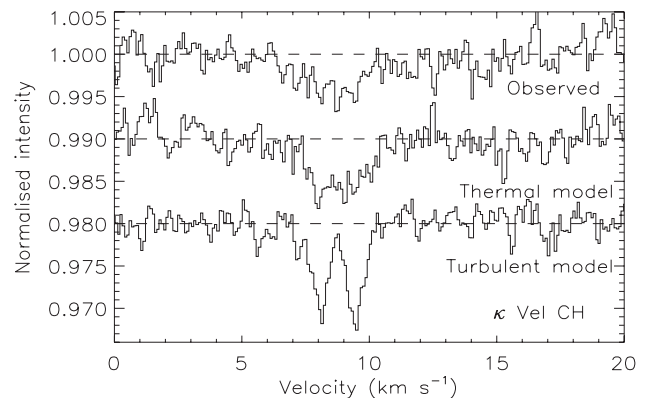
In principle, it should be possible to determine T_k and v_t separately by solving equation (1) for species with differing values of m. However, there are no systematic differences in b values between

species in component B, over a range $m = 23$ (Na I) to $m = 40$ (Ca I and Ca II). In component A, statistically significant differences in b are found between species, but with K I the narrowest and Ca I the broadest. This is difficult to reconcile with equation (1), which implies that the least massive species (Na I) should have the highest b value. The most likely explanation for these discrepancies is that the species are not entirely physically coincident and reside within different parts of the cloud, perhaps in regions with differing v_t. If v_t makes a significant contribution to the b values, then the kinetic temperature could be substantially lower than the derived upper limits.

5.3 CH distribution

Visual inspection of the CH spectrum shows no sign of the expected Λ-doublet line profile, which causes the relatively high value of b in the single-component VAPID model. In order to determine if CH has the same line profile as the atomic species but the Λ-doublet is being hidden by the noise, simulated CH line profiles were constructed. Two components were assumed, with velocity separation and column density ratio equal to that observed in K I, which is known to be distributed similarly to CH in diffuse clouds (e.g. Welty & Hobbs 2001; Pan et al. 2005), and a total column density equal to the CH model. Two limiting cases for b were considered: v_t dominant (the 'turbulent' model, $T_k = 0$) and T_k dominant (the 'thermal' model, $v_t = 0$). For the turbulent model, we assume b values equal to those of K I (Table 3). Because CH ($m = 13$) is substantially less massive than K ($m = 39$), the thermal model adopts b values of 1.06 and 0.60 km s^{-1}, i.e. a factor of $\sqrt{3}$ ($= \sqrt{39/13}$) higher than the turbulent model. These simulated line profiles were then degraded to the obtained noise level using clean sections of the observed continuum near the CH line, which avoids the need to make assumptions about the noise statistics.

The simulated spectra are compared with the observation in Fig. 11. The Λ-doublet is clearly visible in the turbulent model, but barely discernible in the thermal model. A simulation in which only component A is 'turbulent' is not very different from the combined thermal model illustrated: it is the degree of turbulent broadening

Figure 11. Observed and simulated CH line profiles. Upper histogram is the observed CH profile as in Fig. 5, middle histogram is the 'thermal' model, and the lower histogram is the 'turbulent' model, assuming CH shares the same distribution as K I (see Section 5.3 for details of the models). The spectra have been vertically offset by 0.01 for display; the dashed lines illustrate the continuum levels. The observed line profile is significantly broader than the turbulent model, and the Λ-doublet is not visible in the observed spectrum.

in the narrower component B which is primarily constrained by this analysis. It is therefore plausible that the CH shares a similar distribution to K I but the line profile is being masked by noise. If so, the turbulent contribution to the CH line profile is low, at least in component B. This suggests that the temperature of component B cannot be much lower than the upper limit derived in Section 5.2.

We also constructed simulated spectra based on the Ca I distribution, which is more heavily concentrated in component B than K I. In those simulations, the Λ-doublet is clearly visible even in the thermal model, which is inconsistent with the observations. This supports the assumption made above that CH is distributed more similarly to K I than Ca I.

5.4 Ca I/Ca II ratio and electron density

At the low densities prevalent in the diffuse ISM, the balance between the various ionization states of a single atom is set by the competition between photoionization which promotes the atom to a higher ionization state, and recombination with an electron which demotes it to a lower one. For the neutral and first ionized state in equilibrium, this may be expressed as

$$\Gamma(X\,\textsc{i})\,n(X\,\textsc{i}) = \alpha_r(X\,\textsc{i},T)\,n(X\,\textsc{ii})\,n_e\,, \qquad (2)$$

where Γ is the photoionization rate, α_r the radiative recombination rate coefficient, n_e the electron number density and $n(X)$ the number density of species X. As observations provide the column density N and not the number density n, it is necessary to assume a constant density along the line of sight, allowing n to be replaced by N. Under this assumption, and for the specific case of calcium, equation (2) may be rewritten as

$$n_e = \frac{\Gamma(Ca\,\textsc{i})}{\alpha_r(Ca\,\textsc{i},T)}\frac{N(Ca\,\textsc{i})}{N(Ca\,\textsc{ii})}. \qquad (3)$$

Calcium is an unusual case because both its first and second ionization energies (6.11 and 11.87 eV, respectively) are lower than the Rydberg energy (13.6 eV), so in diffuse clouds ionization to Ca III is possible. There is then a second ionization equilibrium between Ca II and Ca III, though this does not invalidate the electron densities derived from equation (3). Welty, Hobbs & Morton (2003) calculated the relative populations of Ca I, Ca II and Ca III and found that the dominant ionization state is Ca II in any situation where Ca I is abundant enough to be detected.

Equation (3) is an approximation which assumes that no other processes cause significant conversion between ionization stages. Plausible processes include cosmic ray ionization and charge exchange with dust grains or polycyclic aromatic hydrocarbons (e.g. Liszt 2003). Welty et al. (2003) have discussed this issue in the context of calcium ionization ratios, and concluded that equation (3) remains valid if the fractional ionization $n_e/n_H \lesssim 2 \times 10^{-4}$, which is the level provided by complete ionization of gas-phase C I to C II (assuming standard depletions, see also Section 5.7). Those authors also conclude that the assumption of photoionization is most valid when n_e is high. Since the observations towards κ Vel indicate a cloud which is much cooler and/or more dense than usual for the diffuse ISM, and as the low extinction present in the cloud[5] favours photoionization, the assumptions leading to equation (3) are expected to be valid in this case.

The electron density may then be determined from the column densities, given the value $\Gamma/\alpha_r = 66$ for Ca I given by Welty et al. (2003, their table 3).[6] The electron densities are then found to be $n_{e,A} = 0.98 \pm 0.12$ cm^{-3} and $n_{e,B} = 3.14 \pm 0.77$ cm^{-3} for components A and B, respectively. These are very high values for diffuse clouds. For comparison, Crawford (2002) found $n_e = 0.97$ cm^{-3} towards κ Vel using a single-component model.

Some observers have found that electron densities derived from calcium are sometimes higher than those derived from other species along the same lines of sight. Welty et al. (1999) used ionization ratios of nine different elements to determine n_e towards 23 Ori, with calcium resulting in the highest estimate, whilst Sonnentrucker et al. (2003) found that calcium gave the highest n_e (out of four measured ionization ratios) towards HD 185418. This effect has only been reported towards a handful of stars, and the cause is unknown (see Welty et al. 2003 for a discussion). There is some circumstantial evidence to support the electron density derived from calcium: the changes seen in K I are about the same rate as those seen in Ca I (Section 5.1), suggesting that both are responding to the same change in (observed) electron density; and the total number densities derived independently from the electron density and the chemical model (Sections 5.7 and 5.9) are in agreement with each other.

5.5 Ca I/K I ratio and depletions

Whilst the Ca I/Ca II ratio provides a measure of the electron density (under the assumption of constant temperature), some line ratios are sensitive to other properties of the interstellar gas. Because the depletion of potassium into dust grains is thought to be fairly constant, the Ca I/K I ratio may be used to estimate the depletion of calcium, which is typically very high at the low temperatures in the diffuse ISM due to its high condensation temperature ($T_C = 1659$ K; Lodders 2003). Welty et al. (2003) found that $N(Ca\,\textsc{i})$ and $N(K\,\textsc{i})$ are correlated, with the slope of that correlation arising from the difference in depletion behaviours. Our measured ratios fall very close to the mean relation determined by Welty et al. (2003), suggesting that there is no unusual enhancement of Ca I along this line of sight. Adopting the same assumptions as for the calcium ionization balance, and assuming that Ca II is dominant, the relative populations of Ca I and K I are given by

$$\frac{N(Ca\,\textsc{i})}{N(K\,\textsc{i})} = \frac{(\Gamma/\alpha_r)_{Ca\,\textsc{i}}}{(\Gamma/\alpha_r)_{K\,\textsc{i}}}\frac{\delta(Ca)a_{Ca}}{\delta(K)a_K}\,, \qquad (4)$$

where $\delta(X)$ is the gas-phase fraction and a_X the cosmic abundance of species X. Taking the standard abundances, $\delta(K) = 0.2$, and photoionization and recombination rates given by Welty et al. (2003), this becomes

$$\frac{N(Ca\,\textsc{i})}{N(K\,\textsc{i})} \approx 12.4\delta(Ca). \qquad (5)$$

This gives estimates of the calcium gas-phase fraction in components A and B of $\delta(Ca)_A = (1.51 \pm 0.23) \times 10^{-2}$ and $\delta(Ca)_B = (7.42 \pm 1.45) \times 10^{-3}$, which may be equivalently expressed as $D(Ca)_A = -1.82 \pm 0.13$ and $D(Ca)_B = -2.13 \pm 0.17$, where D are the logarithmic depletions. Cardelli, Federman & Smith (1991) investigated the depletion of calcium in diffuse clouds, and concluded that it is very sensitive to the local density, increasing in

---

[5] $E(B - V) = 0.10$, so $A_V = 0.16$ halfway through the interstellar material along the line of sight, assuming $R_V = 3.1$. The transverse extinction is unknown but probably even lower.

[6] This value assumes $T = 100$ K. For calcium, the dependence of α_r on T is $\alpha \propto (T/100\,\text{K})^{-0.683}$ (Pequignot & Aldrovandi 1986). Γ is independent of T.

denser regions. This is in accordance with our result of a higher calcium depletion in component B (which is found to be approximately a factor of 2 denser than component A in Section 5.7).

5.6 Molecular hydrogen fraction

The Ca I/K I ratio is also correlated with the fraction of hydrogen in the form of H_2, though the relation is not particularly tight (Welty et al. 2003). Previous observations have only resulted in upper limits for the H I and H_2 column densities towards κ Vel (Jenkins 2009, whose results were based on the observations of Bohlin et al. 1983 corrected for stellar contamination). The measured ratios are $\log(N(\text{Ca I})/N(\text{K I}))_A = -0.729 \pm 0.035$ and $\log(N(\text{Ca I})/N(\text{K I}))_B = -1.036 \pm 0.052$. These correspond to upper limits for the fraction of hydrogen in the form of H_2 of $f(H_2) \lesssim 10^{-2}$ in both components (Welty et al. 2003, their fig. 4). These are very low molecular hydrogen fractions for the diffuse ISM, especially for regions with enhanced density.

A more direct estimate of the molecular hydrogen fraction could in principle be obtained from the standard relations between $E(B - V)$ and H I, and between $N(\text{CH})$ and H_2. Adopting $E(B - V) = 0.10$ (Cha et al. 2000) with an uncertainty[7] of 0.02 mag, equation (7) of Burstein & Heiles (1978) predicts $\log N(\text{H I}) = 20.9 \pm 0.2$. Taking $\log(N(\text{CH})/N(H_2)) = -7.46 \pm 0.21$ from Sheffer et al. (2008),[8] we obtain an estimate of $\log N(H_2) = 18.93 \pm 0.22$. This implies a molecular fraction of $f(H_2) \equiv \frac{2N(H_2)}{N(\text{H I})+2N(H_2)} = (2.1 \pm 1.6) \times 10^{-2}$, which is in line with the previous estimate.

Both of these estimated column densities are more than 1 dex higher than the upper limits from the UV observations (Jenkins 2009). We also note that Welty & Hobbs (2001) presented empirical relations between K I, Na I and total hydrogen column density for typical diffuse ISM lines of sight, but for κ Vel these would again imply at least an order of magnitude more hydrogen than the observed upper limits. Apparently the standard relations are not valid for the line of sight towards κ Vel. It is possible that the column densities have changed by this amount between the epochs of the UV observations (late 1970s; Bohlin et al. 1983) and the optical observations [the $E(B - V)$ measurement is based on Tycho photometry and so has an effective epoch of 1991.5, whilst the spectroscopic measurements are from 2006]. Alternatively, the ISM towards κ Vel could be out of chemical equilibrium (Bell et al. 2005) and thus these standard relations might not apply.

5.7 Physical dimensions and density

The proper motion of κ Vel is 15.5 mas yr^{-1} (Perryman 1997), so at a distance of 165 pc the transverse velocity is 2.56 au yr^{-1} (12.1 km s^{-1}). This gives a stellar displacement of 10.1 au between the 2002 and 2006 observations, and 29.7 au between 1994 and 2006 (shown on the axes of Figs 9 and 10). The size of the binary orbit has been determined to be $a_1 \sin i = 0.48$ au, where a_1 is the semimajor axis of the orbit of the primary and i the orbital inclination (Pourbaix et al. 2004). Since neither the inclination nor position angle of the orbital ellipse has been determined, it is impossible to include the effect of this on the transverse displacement, but the error thus introduced is likely to be rather small.

---

[7] The uncertainty on $E(B - V)$ is taken to be equivalent to a misclassification by one spectral subtype.

[8] Note that this requires extrapolating the Sheffer et al. (2008) relation to lower column densities than they actually observed.

The displacement of the line of sight at the distance of the star provides an upper limit on the displacement at the distance of the foreground absorbing cloud. Dunkin & Crawford (1999) have argued that the cloud is likely to be located close to the star, at least 150 pc from the Sun, based on comparison with CO maps and optical absorption along other nearby lines of sight (see also Crawford 1991). This would place the cloud just beyond the edge of the Local Bubble (Welsh et al. 2010). Any transverse motion of the interstellar cloud would modify the displacement of the line of sight through the cloud by the vector sum of the motions of the star and cloud. It is impossible to determine the transverse velocity of the cloud, but reasonable assumptions suggest that the derived cloud size is accurate to within a factor of 2–3, in either direction.

If the electron density is dominated by electrons released through the photoionization of atomic carbon (the assumption adopted by Crawford 2002), the electron density allows an estimate of the total number density to be obtained. Assuming a carbon depletion of 60 per cent implies a gas-phase carbon abundance of $1.4 \times 10^{-4} n_H$ (Sofia et al. 1997), which leads to estimates of $n_A \gtrsim 7 \times 10^3$ cm^{-3} and $n_B \gtrsim 2 \times 10^4$ cm^{-3}. These are orders of magnitude higher than typical values for diffuse or translucent clouds (Snow & McCall 2006). They are also higher than the densities inferred by some SSS studies (e.g. Pan, Federman & Welty 2001), but those studies relied upon simple chemical models to determine the density. Bell et al. (2005) demonstrated that the chemistry can be time dependent in small-scale structures, whilst the atomic species react much more rapidly to changing conditions.

Welty (2007) combined optical and UV observations (including C I and C II) of the small-scale structure towards HD 219188. It was inferred that the changing column densities reflected enhanced recombination due to a raised electron density, the source of which was the ionization of hydrogen. If this effect is also present in the line of sight towards κ Vel, the densities derived above will be overestimates. Since hydrogen is thousands of times more abundant than carbon, even a small fractional ionization of hydrogen could reduce the density estimate by an order of magnitude or more. An ionization fraction of $\gtrsim 1$ per cent would be required to reduce the density to levels typical of the diffuse ISM. A physical cause for the ionization would also be required, such as intense cosmic ray bombardment or penetration of soft X-rays through the relatively low-extinction gas (Tielens 2005), though the latter might plausibly arise from the hot gas in the Local Bubble (Frisch, Redfield & Slavin 2011).

An estimate of the hydrogen column density may be derived from the observed metal column densities and depletion estimates. Taking $\log[\text{Ca/H}] + 12 = 6.34$ from Asplund et al. (2009), $D(\text{Ca})$ estimates from Section 5.5 and the observed Ca I + Ca II column densities, we obtain $\log N_A(\text{H}) \approx 18.7$ and $\log N_B(\text{H}) \approx 18.3$, so $\log N_{AB}(\text{H}) \approx 18.9$. This is consistent with the observational upper limits of $\log N(\text{H I}) < 19.5$ and $\log N(H_2) < 17.7$ (Jenkins 2009). Taking these column density estimates and assuming a density of 10^4 cm^{-3} gives an estimated total path length of ~ 50 au. This length estimate rests upon a series of assumptions, in particular the derived calcium depletions and neglecting Ca III, so is probably only indicative to within an order of magnitude.

5.8 C_2 column density

The relative populations of the low-J rotational states of C_2 depend upon the local density and kinetic temperature. In order to determine an upper limit on the total C_2 column density, it is necessary to combine the limits on the equivalent width for lines with

differing J derived in Section 4.4 with the density and temperature determinations from Sections 5.2 and 5.7. Since C_2 is expected to preferentially form in denser regions, we adopt $n = 2 \times 10^4$ cm^{-3} and assume $T_k = 100$ K.

The relative populations of each J level were calculated using B. McCall's online calculator,[9] which uses the method of van Dishoeck & Black (1982). The populations of each level were combined with the oscillator strengths from Table 2 and the calculated total population (i.e. integrating over all J) to determine the maximum total column density which is compatible with the equivalent width upper limits. The resulting 2σ upper limit is $N(C_2) \lesssim 5.6 \times 10^{11}$ cm^{-2}.

Adopting a higher density or lower temperature would result in a somewhat tighter upper limit. At $T_k = 100$ K, the calculation is rather insensitive to n: if n changes by an order of magnitude, the calculated upper limit differs by less than 5 per cent. Varying T_k by 20 K changes the upper limit by $\sim$10 per cent.

5.9 Comparison with chemical models

The chemical models of Bell et al. (2005) made predictions for the column densities of CH, C_2, Ca I and Ca II (plus OH and CO) along a line of sight through an SSS filament. The physical parameters were based on those derived by Crawford (2002) for κ Vel, namely an extended structure of length 100 au along the line of sight and transverse depth of 10 au. Results were presented for a grid of cloud densities and times.

Because CH shows no evidence for more than one cloud component and C_2 has only an upper limit over the total line of sight, for comparison with the chemical model column densities were initially summed over both components A and B. The total column densities adopted in this case[10] were $N_{AB}(CH) = 2.95 \times 10^{11}$ cm^{-2}, $N_{AB}(C_2) \lesssim 5.6 \times 10^{11}$ cm^{-2} (2σ), $N_{AB}(Ca I) = 4.17 \times 10^9$ cm^{-2} and $N_{AB}(Ca II) = 2.07 \times 10^{11}$ cm^{-2} (cf. Section 5.1). With the exception of Ca II, these column densities are fully consistent with the Bell et al. results for $n = 5 \times 10^4$ cm^{-3}, $t = 10$–50 yr. Models with $n = 10^5$ cm^{-3} are excluded by the C_2 upper limit, whilst those with lower density are excluded by the Ca I column density. The observed Ca II column density is moderately higher than the model, by a factor of $\sim$4, but this is within the uncertainties of the models.

In an attempt to include material only in the densest regions, we have also compared the Bell et al. (2005) models to component B alone – this component was suspected to be variable by Crawford et al. (2000). It then becomes necessary to assume that all of the CH arises within component B (but see the discussion in Section 4.3), and the high column density of Ca I in component A cannot be explained. Bearing in mind these caveats, the CH and C_2 column densities remain as above, whilst the calcium column densities are $N_B(Ca I) = 1.58 \times 10^9$ cm^{-2} and $N_B(Ca II) = 3.32 \times 10^{10}$ cm^{-2}. All the observed column densities are then consistent with the Bell et al. model for $n = 5 \times 10^4$ cm^{-3}, $t = 10$ yr.

The chemical models thus provide confirmation of the high number density in the cloud towards κ Vel, and are most consistent with densities only slightly higher than the lower limits derived in Section 5.7. The predicted C_2 column density in the most consistent model is roughly a factor of 3 times lower than our observed upper limit. The models determined the local temperature through a self-consistent treatment of heating and cooling processes. The

range of temperatures in the models was $\sim$30–115 K, which are consistent with the upper limits derived in Section 5.2. It is difficult to interpret the time-dependent aspect of the models, because the structure cannot have formed instantaneously. Nevertheless, the models predict that for $n = 5 \times 10^4$ cm^{-3} CH and Ca II would be essentially constant over time, whilst Ca I would increase, as observed (cf. Fig. 10).

Bell et al. set $n(H_2)/n(H I) = 0.4$, which is more than an order of magnitude higher than the molecular hydrogen fraction inferred in Section 5.6. Low molecular hydrogen fractions would act to reduce the column densities of the molecular species because the formation pathways all include reactions with H_2. The estimates in Section 5.6 might therefore be misleading, as the correlations may not hold in such high-density regions. Alternatively, the local density and/or H_2 fraction could be highly variable along the line of sight. A large number of such variations in local density (and to an extent temperature) have been proposed by Cecchi-Pestellini et al. (2009) as a solution to several problems in diffuse cloud chemistry. If this were the case, it would be possible for CH to be formed in regions of relatively high H_2 density, but for the atomic lines to trace less dense material elsewhere, therefore reducing the total molecular fraction along the line of sight. In the absence of direct observations, this contradiction in $f(H_2)$ cannot currently be resolved.

5.10 Diffuse interstellar bands

The measured DIB equivalent widths are far lower than expected given the reddening, and only a few DIBs have been detected. Based on 133 lines of sight, Friedman et al. (2011) found a mean $W(\lambda 5780)/E(B - V)$ value of 505 mÅ mag^{-1}. However, towards κ Vel, the reddening is $E(B - V) = 0.10 \pm 0.02$ but $W(\lambda 5780)$ is 10 ± 1 mÅ, i.e. five times lower than would be typical for the Milky Way ISM. The relative weakness of $\lambda 5780$ indicates a lower abundance of its carrier in the dense material towards κ Vel than in the ambient ISM, which may indicate a density dependence of the (unknown) carrier formation mechanism.

Those DIBs which have been detected towards κ Vel are members of Krełowski & Walker (1987) group 2, whilst the DIBs of group 3 are absent. The equivalent width ratio of $\lambda 5780$ (a group 2 DIB) to $\lambda 5797$ (group 3) is at least $W(\lambda 5780)/W(\lambda 5797) > 22$ (1σ), which is amongst the highest known: typical values of this ratio are 1–4. As far as the authors are aware, the highest ratios previously reported in the literature are $W(\lambda 5780)/W(\lambda 5797) > 9$ (1σ) towards the star ϵ Cassiopeiae by Friedman et al. (2011), and $W(\lambda 5780)/W(\lambda 5797) = 8.2$ (no uncertainty given) towards HD 20336 by Galazutdinov et al. (1998).[11] Krełowski et al. (1999) found a correlation between $W(\lambda 5797)/W(\lambda 5780)$ and $W(CH)/E(B - V)$. Although the value of $W(CH)/E(B - V) = 2.5 \pm 0.6$ mÅ mag^{-1} measured towards κ Vel is much lower than any measured by Krełowski et al., the upper limit on $W(\lambda 5797)/W(\lambda 5780)$ does appear to fall on or near this relation.

The observed $\lambda 5780/\lambda 5797$ ratio corresponds to a cloud of extreme σ-type (Krełowski et al. 1992), which is generally interpreted as a low density, high UV radiation field environment. The additional DIBs and diatomic molecules present in ζ-type

---

[9] http://dib.uiuc.edu/c2
[10] Although components A and B were not observed in CH and C_2, we assume that these molecules are confined to those cloud components.

[11] Porceddu, Benvenuti & Krełowski (1992) report five sightlines with high $\lambda 5780/\lambda 5797$ ratios, and Galazutdinov et al. (1998) three more, but neither set of authors report the value of the ratio nor provide numerical upper limits on $W(\lambda 5797)$.

clouds (generally interpreted as cooler, denser and less UV irradiated than σ-type) are extremely weak or absent. However, the analysis above indicates that the interstellar cloud(s) towards κ Vel is/are relatively dense but unshielded from UV radiation. The weakness of λ5780 with respect to $E(B - V)$ and the extreme σ-type line of sight suggests that unusual conditions are present in the cloud towards κ Vel. Cami et al. (1997) found similar properties [weak DIBs per unit $E(B - V)$, extreme λ5780 to λ5797 ratio, weak or absent diatomics] towards targets in Orion, where the conditions are also fairly dense but highly UV irradiated. Snow et al. (1995) found systematically weak DIBs in reflection nebulae, where conditions are even more extreme in terms of high UV field and high electron density.

It has been suggested that the carrier of the λ5797 DIB is a neutral species which is easily ionized, whilst the λ5780 carrier does not easily change ionization state due to being either an already ionized species or a neutral which is highly resistant to ionization (e.g. Cami et al. 1997; Krełowski, Galazutdinov & Musaev 1998).[12] Because the λ5780 intensity over a large sample correlates very well with $N(\text{H\,\sc{i}})$, it has also been suggested that the carrier has an ionization energy similar to that of hydrogen (Friedman et al. 2011). Whilst the hypothesis on the nature of the λ5797 carrier is in accordance with the widely observed enhancement of λ5797 in less UV-irradiated environments, it appears to be at odds with the lack of λ5797 detection towards κ Vel given the high electron densities derived in Section 5.4.

High electron densities should lead to enhanced recombination of molecular cations to form neutral molecules, as well as the observed neutral atomic species. However, this would result in relatively strong λ5797, opposite to what is observed towards κ Vel. Electronic recombination with a molecular cation does not necessarily produce the neutral through radiative association because the molecule may lose energy through fragmentation instead of emitting a photon. But if such fragmentation pathways are significant for the carrier of λ5797, this should result in *destruction* of the carrier in environments with high electron density; this is incompatible with the hypothesized enhancement of λ5797 in dense environments due to enhanced recombination of a cation.

It appears that the carrier of the λ5797 DIB (and, by extension, the other DIBs in Krełowski & Walker group 3) is more sensitive to UV irradiation than density or degree of ionization. The observations of κ Vel may indicate that the carrier of λ5797 is dissociated by UV radiation more rapidly than the carrier of λ5780.

Although the K\,\sc{i} line was not observed in 1995, by interpolating Fig. 9 it is inferred that the equivalent width of the K\,\sc{i} line increased by $\approx$80 per cent between the 1995 and 2004 observations; the limit on the change in λ5780 DIB is $\lesssim$40 per cent. If the carrier of λ5780 were to have increased in proportion with the K\,\sc{i} line, a change would have been seen between 1995 and 2004, albeit with low statistical significance. Cordiner et al. (2006) and Cordiner et al. (in preparation) found that DIB carriers (including λ5780) trace the same SSS as atomic lines such as K\,\sc{i}. The fairly loose upper limit on the variation of λ5780 towards κ Vel is insufficient to draw firm conclusions on this point.

6 CONCLUSIONS

New ultra-high resolution observations of interstellar absorption towards κ Vel by the species K\,\sc{i}, Na\,\sc{i}, Ca\,\sc{i}, Ca\,\sc{ii} and CH have

---

[12] Snow et al. (1995) argued against already ionized species, instead favouring neutral molecules.

been obtained. A search for C_2 was undertaken, but no lines were detected. Best-fitting model line profiles were computed and two main narrow ($b < 0.8$ km s^{-1}) absorption components were identified. Comparisons with observations taken at earlier epochs show increases in interstellar K\,\sc{i} and Ca\,\sc{i} column densities over a period of several years. Since the previous observations in 2002, the transverse velocity of the star has shifted the line of sight through the interstellar cloud by $\sim$10 au.

From a consideration of the Doppler b parameter in each component, a rigorous upper limit was placed on the kinetic temperature of each component. Combining limits from each species, the temperatures of components A and B must be $T_{k,A} < 671^{+18}_{-17}$ and $T_{k,B} < 114^{+15}_{-14}$ K. However, the temperatures may be lower if the turbulent velocity makes a significant contribution to the b values. The Ca\,\sc{i}/K\,\sc{i} ratio was used to derive logarithmic depletions of $D(\text{Ca})_A = -1.82$ and $D(\text{Ca})_B = -2.13$.

The Ca\,\sc{i}/Ca\,\sc{ii} ratio was used to derive estimates of the electron density in the two components. By assuming that electrons originate from photoionization of neutral atomic carbon and assuming a value of 60 per cent for the carbon depletion, lower limits on the density of $n_A \gtrsim 7 \times 10^3$ cm^{-3} and $n_B \gtrsim 2 \times 10^4$ cm^{-3} were derived. These values are far higher than typical densities in the diffuse ISM. Comparison of the observations with the chemical model of Bell et al. (2005) confirms the requirement for a high number density, with $n = 5 \times 10^4$ cm^{-3} in the best-fitting model.

The first detections of DIBs towards κ Vel were made at two epochs, but only a loose upper limit of $\lesssim$40 per cent could be placed on the variation of DIB absorption between the two epochs. The DIBs detected are weak given the measured $E(B - V)$, and an unusually high λ5780/λ5797 ratio of $>$22 was found, amongst the highest known. This suggests that the carrier of λ5797 is more sensitive to UV radiation than local density. The behaviour of DIBs towards κ Vel appears to be similar to that observed in Orion by Cami et al. (1997). The weakness of the DIBs [per unit $E(B - V)$] may be related to the high density of the material towards κ Vel.

Continued monitoring of interstellar absorption lines towards κ Vel would be of interest, in order to determine the size of the structure from the time taken for the column density to peak and subsequently decline. It would be beneficial to observe the C\,\sc{i} fine structure lines in the UV to allow derivation of the local density and kinetic temperature. Although this approach leads to some degeneracy in these parameters, this could be lifted via the existing constraints on temperature and density, though (nearly) simultaneous optical observations would be an advantage. A direct measurement of the H_2 fraction would also be beneficial.

REFERENCES

Andrews S. M., Meyer D. M., Lauroesch J. T., 2001, ApJ, 552, L73
Asplund M., Grevesse N., Sauval A. J., Scott P., 2009, ARA&A, 47, 481

Bell T. A., Viti S., Williams D. A., Crawford I. A., Price R. J., 2005, MNRAS, 357, 961

Black J. H., van Dishoeck E. F., 1988, ApJ, 331, 986

Blades J. C., Sahu M. S., He L., Crawford I. A., Barlow M. J., Diego F., 1997, ApJ, 478, 648

Bohlin R. C., Jenkins E. B., Spitzer L., York D. G., Hill J. K., Savage B. D., Snow T. P., 1983, ApJS, 51, 277

Burstein D., Heiles C., 1978, ApJ, 225, 40

Cami J., Sonnentrucker P., Ehrenfreund P., Foing B. H., 1997, A&A, 326, 822

Cardelli J. A., Federman S. R., Smith V. V., 1991, ApJ, 381, L17

Cecchi-Pestellini C., Williams D. A., Viti S., Casu S., 2009, ApJ, 706, 1429

Cha A. N., Sahu M. S., Moos H. W., Blaauw A., 2000, ApJS, 129, 281

Cordiner M. A., 2006, PhD thesis, The University of Nottingham

Cordiner M. A., Fossey S. J., Smith A. M., Sarre P. J., 2006, Faraday Discussions, 133, 403

Crane P., Lambert D. L., Sheffer Y., 1995, ApJS, 99, 107

Crawford I. A., 1991, A&A, 247, 183

Crawford I. A., 1997, MNRAS, 290, 41

Crawford I. A., 2002, MNRAS, 334, L33

Crawford I. A., 2003, Ap&SS, 285, 661

Crawford I. A., Howarth I. D., Ryder S. D., Stathakis R. A., 2000, MNRAS, 319, L1

Crovisier J., Kazes I., Dickey J. M., 1985, A&A, 146, 223

Danks A. C., Walborn N. R., Vieira G., Landsman W. B., Gales J., García B., 2001, ApJ, 547, L155

Diamond P. J., Goss W. M., Romney J. D., Booth R. S., Kalberla P. M. W., Mebold U., 1989, ApJ, 347, 302

Diego F. et al., 1995, MNRAS, 272, 323

Dieter N. H., Welch W. J., Romney J. D., 1976, ApJ, 206, L113

Dunkin S. K., Crawford I. A., 1999, MNRAS, 302, 197

Frail D. A., Weisberg J. M., Cordes J. M., Mathers C., 1994, ApJ, 436, 144

Friedman S. D. et al., 2011, ApJ, 727, 33

Frisch P. C., Redfield S., Slavin J. D., 2011, ARA&A, 49, 237

Galazutdinov G. A., Krełowski J., Moutou C., Musaev F. A., 1998, MNRAS, 295, 437

Głebocki R., Stawikowski A., 2000, Acta Astron., 50, 509

Hartquist T. W., Falle S. A. E. G., Williams D. A., 2003, Ap&SS, 288, 369

Heiles C., 1997, ApJ, 481, 193

Heiles C., 2007, in Haverkorn M., Goss W. M., eds, ASP Conf. Ser. Vol. 365, SINS - Small Ionized and Neutral Structures in the Diffuse Interstellar Medium. Astron. Soc. Pac., San Francisco, p. 3

Heiles C., Stinebring D., 2007, in Haverkorn M., Goss W. M., eds, ASP Conf. Ser. Vol. 365, SINS - Small Ionized and Neutral Structures in the Diffuse Interstellar Medium. Astron. Soc. Pac., San Francisco, p. 331

Hobbs L. M. et al., 2008, ApJ, 680, 1256

Howarth I. D., Price R. J., Crawford I. A., Hawkins I., 2002, MNRAS, 335, 267

Jenkins E. B., 2009, ApJ, 700, 1299

Jenkins E. B., Tripp T. M., 2001, ApJS, 137, 297

Jenkins E. B., Tripp T. M., 2011, ApJ, 734, 65

Krełowski J., Walker G. A. H., 1987, ApJ, 312, 860

Krełowski J., Snow T. P., Seab C. G., Papaj J., 1992, MNRAS, 258, 693

Krełowski J., Galazutdinov G. A., Musaev F. A., 1998, ApJ, 493, 217

Krełowski J., Ehrenfreund P., Foing B. H., Snow T. P., Weselak T., Tuairisg S. Ó., Galazutdinov G. A., Musaev F. A., 1999, A&A, 347, 235

Lazio T. J. W., Brogan C. L., Goss W. M., Stanimirović S., 2009, AJ, 137, 4526

Liszt H., 2003, A&A, 398, 621

Lodders K., 2003, ApJ, 591, 1220

McKee C. F., Ostriker J. P., 1977, ApJ, 218, 148

Meyer D. M., 1990, ApJ, 364, L5

Morton D. C., 2003, ApJS, 149, 205

Pan K., Federman S. R., Welty D. E., 2001, ApJ, 558, L105

Pan K., Federman S. R., Sheffer Y., Andersson B.-G., 2005, ApJ, 633, 986

Pequignot D., Aldrovandi S. M. V., 1986, A&A, 161, 169

Perryman M. A. C., ed., 1997, ESA SP-1200, The HIPPARCOS and TYCHO Catalogues. Astrometric and Photometric Star Catalogues Derived from the ESA HIPPARCOS Space Astrometry Mission. ESA Publications Division, Noordwijk

Porceddu I., Benvenuti P., Krełowski J., 1992, A&A, 260, 391

Pourbaix D. et al., 2004, A&A, 424, 727

Price R. J., Crawford I. A., Barlow M. J., 2000, MNRAS, 312, L43

Sarre P. J., 2006, J. Molecular Spectrosc., 238, 1

Sheffer Y., Rogers M., Federman S. R., Abel N. P., Gredel R., Lambert D. L., Shaw G., 2008, ApJ, 687, 1075

Smith K. T., 2010, PhD thesis, The University of Nottingham

Snow T. P., McCall B. J., 2006, ARA&A, 44, 367

Snow T. P., Bakes E. L. O., Buss R. H., Seab C. G., 1995, A&A, 296, L37

Sofia U. J., Cardelli J. A., Guerin K. P., Meyer D. M., 1997, ApJ, 482, L105

Sonnentrucker P., Friedman S. D., Welty D. E., York D. G., Snow T. P., 2003, ApJ, 596, 350

Sonnentrucker P., Welty D. E., Thorburn J. A., York D. G., 2007, ApJS, 168, 58

Stanimirović S., Weisberg J. M., Hedden A., Devine K. E., Green J. T., 2003, ApJ, 598, L23

Stanimirović S., Weisberg J. M., Pei Z., Tuttle K., Green J. T., 2010, ApJ, 720, 415

Tielens A. G. G. M., 2005, The Physics and Chemistry of the Interstellar Medium. Cambridge Univ. Press, Cambridge

van Dishoeck E. F., Black J. H., 1982, ApJ, 258, 533

van Leeuwen F., 2007, A&A, 474, 653

van Loon J. T., Smith K. T., McDonald I., Sarre P. J., Fossey S. J., Sharp R. G., 2009, MNRAS, 399, 195

Watson J. K., Meyer D. M., 1996, ApJ, 473, L127

Welsh B. Y., Lallement R., Vergely J.-L., Raimond S., 2010, A&A, 510, A54

Welty D. E., 2007, ApJ, 668, 1012

Welty D. E., Hobbs L. M., 2001, ApJS, 133, 345

Welty D. E., Hobbs L. M., Kulkarni V. P., 1994, ApJ, 436, 152

Welty D. E., Hobbs L. M., Lauroesch J. T., Morton D. C., Spitzer L., York D. G., 1999, ApJS, 124, 465

Welty D. E., Hobbs L. M., Morton D. C., 2003, ApJS, 147, 61

This paper has been typeset from a TEX/LATEX file prepared by the author.